

Article

Microstructure and Wear Resistance of Ti_5Si_3/Ti_3Al Composite Coatings Prepared by Laser Cladding on TA2 Titanium Alloy

Kaijin Huang ^{1,2,*}  and Wanxia Huang ¹

¹ State Key Laboratory of Materials Processing and Die & Mould Technology, Huazhong University of Science and Technology, Wuhan 430074, China; hwx sophia948@163.com

² State Key Laboratory of Advanced Technology for Materials Synthesis and Processing, Wuhan University of Technology, Wuhan 430070, China

* Correspondence: huangkaijin@hust.edu.cn; Tel.: +86-027-87543676

Abstract: In order to improve the wear resistance of titanium alloy, a Ti_5Si_3/Ti_3Al composite coating with improved wear resistance was successfully prepared by laser cladding TA2 titanium alloy using the double-layer presetting method of Ti-63 wt.% Al mixed powder layer/Si powder layer. The microstructure, phase composition and wear resistance of the coating were studied using X-ray diffraction (XRD), scanning electron microscopy (SEM) and pin-disk friction and wear method. The results show that the coating is mainly composed of the Ti_5Si_3 primary phase and Ti_5Si_3/Ti_3Al eutectic structure. The microhardness of the coating is higher than that of the matrix. The average microhardness of the coating is about 668 HV_{0.1}, which is 3.34 times that of the matrix. The coating significantly improves the wear resistance of the TA2 matrix, and the mass wear rate is 1/5.79 of that of the TA2 matrix. The main wear mechanisms of the coating are abrasive wear, adhesive wear and oxidative wear, whereas the main wear mechanisms of the TA2 matrix are adhesive wear and oxidative wear.

Keywords: laser cladding; Ti_5Si_3/Ti_3Al composite coatings; wear resistance; TA2 titanium alloy



Citation: Huang, K.; Huang, W. Microstructure and Wear Resistance of Ti_5Si_3/Ti_3Al Composite Coatings Prepared by Laser Cladding on TA2 Titanium Alloy. *Lubricants* **2023**, *11*, 213. <https://doi.org/10.3390/lubricants11050213>

Received: 11 April 2023

Revised: 3 May 2023

Accepted: 5 May 2023

Published: 9 May 2023



Copyright: © 2023 by the authors. Licensee MDPI, Basel, Switzerland. This article is an open access article distributed under the terms and conditions of the Creative Commons Attribution (CC BY) license (<https://creativecommons.org/licenses/by/4.0/>).

1. Introduction

Titanium alloy has the advantages of low density, high specific strength and strong corrosion resistance, and has broad application prospects in aerospace, ocean engineering, medical devices and other fields. However, the low hardness and poor wear resistance of titanium alloy significantly restrict its service life under frictional conditions. In order to overcome the weakness of low hardness and poor wear resistance of titanium alloy, surface modification technology is widely used to prepare the coating on titanium alloy to improve the wear resistance of titanium alloy. At present, the commonly used surface modification technologies include ion implantation [1], plasma spraying [2,3], vapor deposition [4,5], micro-arc oxidation [6], laser alloying [7], laser cladding [8,9], etc. Among them, laser cladding is of high significance because of its advantages of metallurgical bonding with the matrix and adjustable coating thickness.

Based on the literature, it is known that two methods, namely, the powder presetting method [10–20] and the powder feeding method [7,9,21–24], are mainly used in the laser surface modification of titanium alloy. Among them, powder presetting methods reported in the literature all used single pure powder or mixed powder for one-time presetting, and there are no reports in the literature on the layered presetting method adopted in this paper. For users who cannot afford a laser cladding powder delivery system but need a laser cladding multi-component powder system, using the layered preset powder layer method can reduce the time of pre-mixing powder and improve work efficiency. Therefore, it is necessary to carry out the feasibility of the layered preset powder layer method. This is the purpose and significance of this paper. The hardness and wear resistance of the coating are greatly improved [8–13,15,17–23]. Ti-Al intermetallic compounds [19] and

Ti_5Si_3 silicide [25,26] formed by laser surface modification of Al and Si elements have excellent wear resistance. The wear mechanisms of the coating and substrate are mainly abrasive wear and adhesive wear, respectively [27]. In addition, Ti_5Si_3 has a high melting point, low density, high hardness and good chemical inertness, whereas Ti_3Al and TA2 titanium alloy have similar thermal expansion coefficients and melting points. Therefore, as long as the ratio of Ti_5Si_3/Ti_3Al is appropriate, it is possible to obtain composite coatings with higher temperature resistance, wear resistance and corrosion resistance than the TA2 titanium alloy.

In this paper, a Ti_5Si_3/Ti_3Al composite coating (which refers to the composite coating mainly composed of Ti_5Si_3 and Ti_3Al phases with high hardness) was prepared on TA2 titanium alloy by laser cladding based on the layered presetting powder method, and the microstructure, phase composition and wear resistance of the coating were studied.

2. Materials and Methods

TA2 titanium alloy was selected as the matrix material, and its specific chemical composition is shown in Table 1. The TA2 titanium alloy with dimensions of 100 mm × 50 mm × 10 mm was selected as the substrate for laser cladding. The substrate was sanded and ultrasonically cleaned with ethanol before the powder was preset.

Table 1. Chemical composition of TA2 (wt.%).

Element	Fe	Si	C	N	H	O	Ti
Content	0.2	0.1	0.1	0.05	0.015	0.1	Bal.

Al powder, Si powder and Ti powder with purity of 99.0 wt.% were selected as laser cladding powder materials in this paper. The powder layer was preset as shown in Figure 1. The thickness of each layer was about 0.4 mm, and the total thickness was about 0.8 mm. The binder used was 4 wt.% polyvinyl alcohol (PVA) aqueous solution. In order to ensure the homogeneity of Ti-63 wt.% Al mixed powder, the process of pre-ball milling was adopted in this paper. The specific parameters of the ball milling were as follows. The XQM-1.2L planetary ball milling produced by Xi'an Liyou Mechanical Equipment Co., Ltd., (Xi'an, China) was used; the weight ratio of the agate ball to powder was 6:1; the rotation speed of the ball milling was 180 r/min; and the ball milling time was 2 h.

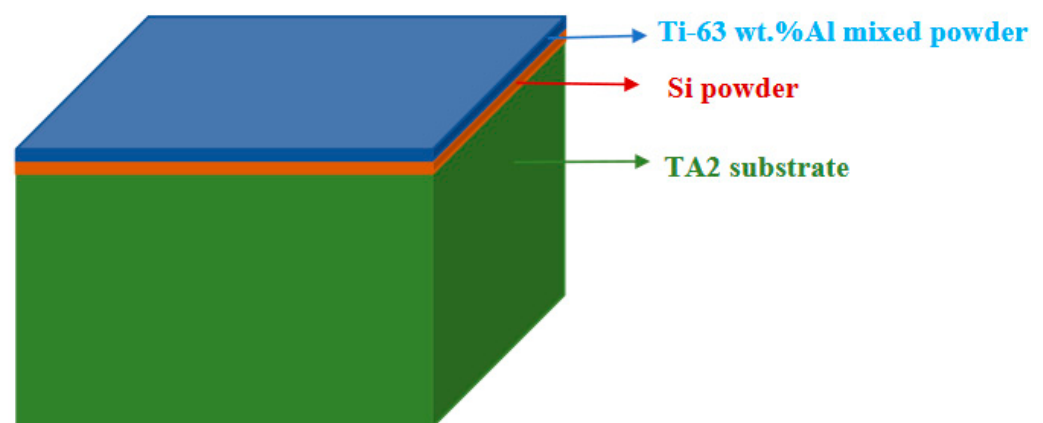


Figure 1. Schematic diagram of presetting powder layer.

Laser cladding was carried out using a Rofin 4 KW fiber laser produced by Rofin Laser Technology Co., Ltd. (Hamburg, Germany). During the laser cladding, argon gas with a purity of 99.999% was used as a protective gas to prevent oxygen in the air from entering the laser molten pool. After several laser cladding parameters were explored, the following optimized laser cladding parameters were finally adopted: laser power $P = 1$ KW; laser

scanning speed $V = 10 \text{ mm/s}$; laser spot diameter $D = 2 \text{ mm}$; the overlapping rate of the laser spot $f = 35\%$; Ar gas flow rate $V_g = 16 \text{ L/min}$.

After laser cladding, the coating and TA2 substrate were cut into $9 \text{ mm} \times 9 \text{ mm} \times 10 \text{ mm}$ samples using the wire cutting method, which were mainly used for the XRD phase composition test, SEM microstructure observation, coating microhardness test and wear resistance test. After wire cutting, all samples were cleaned ultrasonically, dried in a drying oven and then placed in a drying dish for later use. An HVS-1000A microhardness tester produced by Laizhou Huayin Test Instrument Co., Ltd., (Laizhou, China) was used to test the microhardness of the cross-section of the coating. The test parameters were as follows: a load of 100 g and a loading time of 15 s. Finally, the relationship curve between the microhardness HV and surface depth h was drawn according to the microhardness values at different depths.

The wear resistance of the coating and TA2 matrix was tested based on the principle of pin-disk friction and wear tests. The size of the wear sample was $9 \text{ mm} \times 9 \text{ mm} \times 10 \text{ mm}$. The wear device model was Ecomet300/Automet300. The parameters of the dry sliding friction and wear (Figure 2) were as follows: the rotary speed was 200 r/min, the applied load was 45 N, the dry sliding speed was 0.921 m/s, the dry sliding wear time was 5 min, the total wear distance was 276.32 m, and the grinding material was 200# SiC sandpaper. The mass of the samples before and after wear was measured using an SOP Quintix124-1CN electronic analysis balance, and the morphology of the wear was observed using SEM to study the wear mechanism of the coating and substrate.

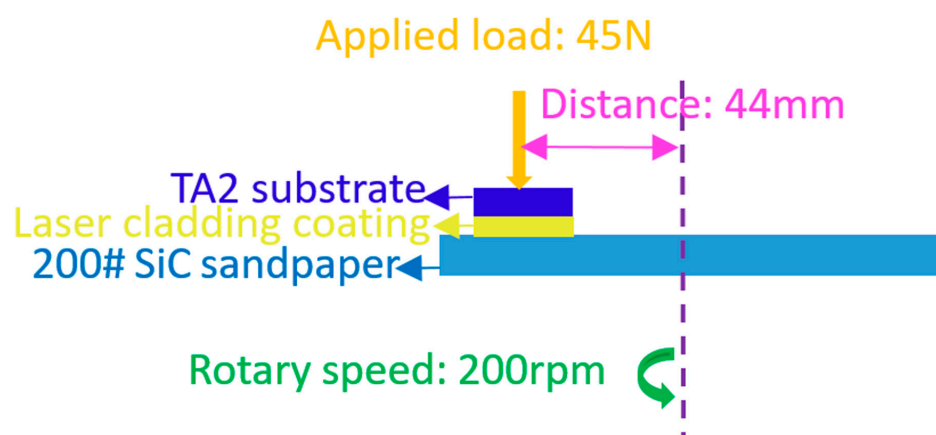


Figure 2. Schematic diagram of dry friction and wear experiment of laser cladding coating.

Phase analysis was performed on the X 'Pert PRO type X-ray diffractometer produced by PANalytical B.V. in the Netherlands (Almelo, The Netherlands). The test conditions were as follows: Cu target, wavelength $\lambda = 0.15406 \text{ nm}$, tube pressure 40 kV, tube flow 40 mA, and 2θ scanning range of $10^\circ \sim 90^\circ$. The microstructure of the coating was observed using a ZEISS SIGMA HD scanning electron microscope made by Carl Zeiss (Jena, Germany). The micromorphology of the worn coating and TA2 matrix was observed using a JSM-7600F scanning electron microscope produced by JEOL (Akishima, Tokyo). The cross-section of the laser cladding coating should be inlaid, ground, polished and etched before the morphology analysis. The composition and proportion of the etching liquid used were HF:HNO₃:H₂O = 7:43:50 (volume ratio), and the etching time was 5~10 s.

3. Results

3.1. Microstructure of the Laser Cladding Coating

Figure 3 shows the XRD pattern of the laser cladding coating. It can be seen from the figure that the laser cladding coating is mainly composed of Ti₃Al (JCPDS 00-052-0859) and Ti₅Si₃ (JCPDS 03-065-3597). The formation of these two phases is undoubtedly very favorable for improving the wear resistance of laser cladding coating because the hardness

of Ti_3Al and Ti_5Si_3 is 5.2 GPa and 11.3 GPa, respectively, both of which are higher than that of Ti (2 GPa). In the laser cladding process, the preset Si powder layer and Ti-63 wt.% Al mixed powder layer melts under the laser and reacts in situ with the partially melted matrix Ti to form Ti_5Si_3 ($5Ti + 3Si = Ti_5Si_3$) and Ti_3Al ($3Ti + Al = Ti_3Al$). According to the calculation results of Zhang [28], the above two reactions in the temperature range of 300–1500 K, ΔG and ΔH are negative. In terms of thermodynamics, a negative ΔH indicates that these two reactions are exothermic and a negative ΔG indicates that these two reactions can occur spontaneously.

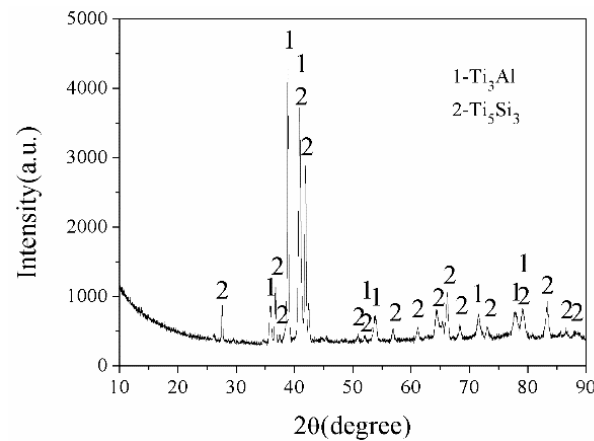


Figure 3. XRD pattern of the laser cladding coating.

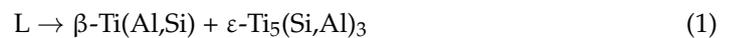
Figure 4a shows the overall morphology of the cross-section coating. It can be seen from the figure that the thickness of the laser cladding layer is about 1 mm. There is a metallurgical bonding between the laser cladding layer and matrix, and no obvious porosity or cracks appear in the coating. Figure 4b–d show the amplified SEM morphologies of the different parts in Figure 4a. According to EDS results (Table 2) and XRD calibration results (Figure 3), it can be determined that the large black block in the coating is the primary Ti_5Si_3 phase, and the rest microstructure is a typical Ti_3Al - Ti_5Si_3 eutectic structure. There are more primary Ti_5Si_3 near the top and middle of the coating (point 1 in Figure 4b and point 3 in Figure 4c), whereas the primary Ti_5Si_3 near the bottom of the coating is less and even completely becomes Ti_3Al - Ti_5Si_3 eutectic structure (point 5 in Figure 4d). This type of microstructure is consistent with those reported by Vojtěch et al. [29] and Wu et al. [30]. Moreover, the components of Al, Si and Ti (see Table 1) also fall within the range of hypereutectic components of Ti_3Al - Ti_5Si_3 reported in the literature [30–32].

Table 2. EDS results of the cross-section coating at different points.

Different Points	Ti (at.%)	Al (at.%)	Si (at.%)	Possible Phases
1	60.79	4.83	34.38	Ti_5Si_3
2	70.00	19.82	10.18	Ti_5Si_3/Ti_3Al
3	61.23	4.70	34.07	Ti_5Si_3
4	78.83	12.18	8.99	Ti_5Si_3/Ti_3Al
5	75.06	19.72	5.22	Ti_5Si_3/Ti_3Al

The solidification process is as follows. After a high-power laser is applied to Ti-63 wt.% Al mixed powder layer and Si powder layer, Ti-63 wt.% Al mixed powder, Si powder and part of the Ti matrix melt after absorbing the laser energy. The three kinds of melts are mixed under the action of the stirring force of a molten pool. When the high-power laser leaves, the molten melt in the molten pool begins to solidify. First, the Ti_5Si_3 phase

with a high melting point crystallizes, forming the primary Ti_5Si_3 phase. With a decrease in temperature, a high-temperature eutectic reaction occurs in the remaining liquid phase [29]:



As the temperature continues to decrease, an isomeric transformation occurs in phase $\beta-Ti(Al,Si)$ [29]:



When the temperature continues to decrease, an ordered reaction occurs in phase $\alpha-Ti(Al,Si)$ [29]:



Thus, when the temperature is lowered to room temperature, the resulting structure is the primary Ti_5Si_3 phase and $\alpha_2-Ti_3(Al,Si) + \varepsilon-Ti_5(Si,Al)_3$ is the eutectic structure.

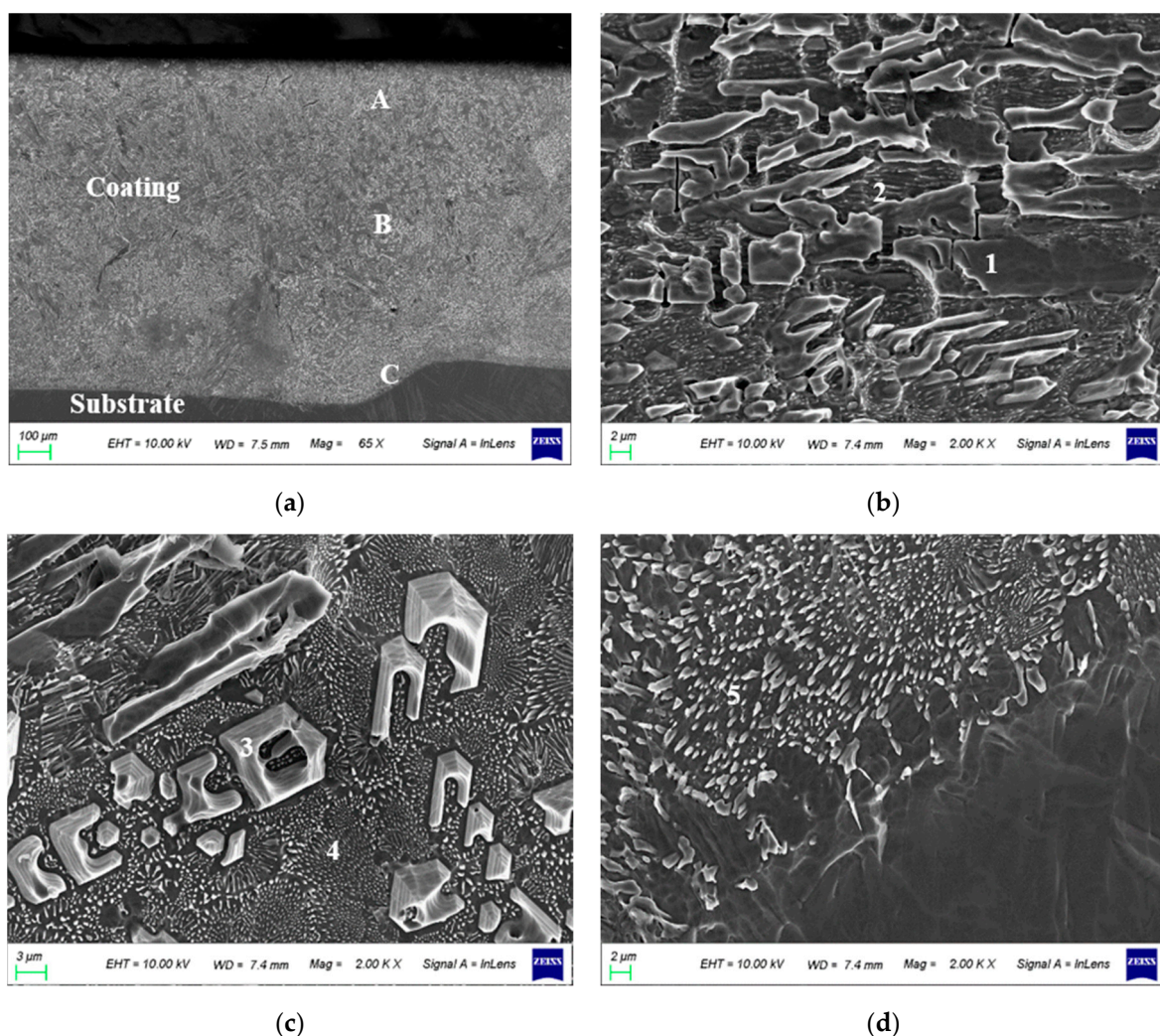


Figure 4. SEM morphology of the cross-section coating: (a) whole; (b) locally amplified at position A in (a); (c) locally amplified at position B in (a); (d) locally amplified at position C in (a). 1, 2, 3, 4 and 5 in figure represent the location points of the EDS test, respectively.

It should be pointed out that in the literature [28], a single-layer presetting method was adopted to laser cladding Ti, Al and Si mixed powders on Ti-6Al-4V titanium alloy, where the thickness of the presetting powder was 0.6~0.8mm. The prepared coating was mainly composed of Ti_5Si_3 , $Ti_7Al_5Si_{12}$, Ti_3AlC_2 , Ti_3Al , $TiAl$, $TiAl_3$ and $\alpha-Ti$, which is much more

complex than the coating prepared by the double-layer presetting method in this paper. This may be related to the flow regularity of Ti, Si and Al powders during the laser action. During the process of laser action, there is a large temperature gradient on the upper and lower surfaces of the molten pool, thus forming a very steep surface tension. The surface tension causes a strong convection in the molten pool, and the convection in the molten pool can produce a strong stirring force so that the liquid metal in the molten pool is mixed evenly. Convection in the molten pool mainly comes from three aspects. First, convection in the molten pool comes from the energy distribution of the laser beam. The Gaussian laser beam used in this experiment can cause severe convection in the molten pool [33]. The second factor is the protective gas blown out in order to prevent the oxidation of the liquid metal at high temperatures. This high-pressure protective gas can produce a certain stirring effect and promote the diffusion of the liquid metal. Third, at high temperatures, the thermal expansion of liquid metal causes a certain density difference in the molten pool, so buoyancy is generated in the molten pool, and the existence of buoyancy causes natural convection of the melt [34]. These three factors that make the layer preset powder can also form a single-layer preset powder structure to reduce the powder mixing time and improve production efficiency.

3.2. Wear Properties of the Laser Cladding Coating

Figure 5 shows the microhardness distribution of the laser cladding coating. As can be seen from the figure, the average microhardness of the coating is about 668 HV_{0.1}, which is 3.34 times that of the TA2 matrix (200 HV_{0.1}). Since the microhardness of Ti₅Si₃ and Ti₃Al is 1500 HV [28] and 530 HV_{0.2} [35], respectively, the microhardness of the laser cladding coating is mainly due to the existence of these harder intermetallic compounds (Figure 3) and fine-grain strengthening due to rapid solidification during laser cladding. Obviously, an increase in the microhardness of the coating is beneficial to the improvement of the wear resistance of the coating.

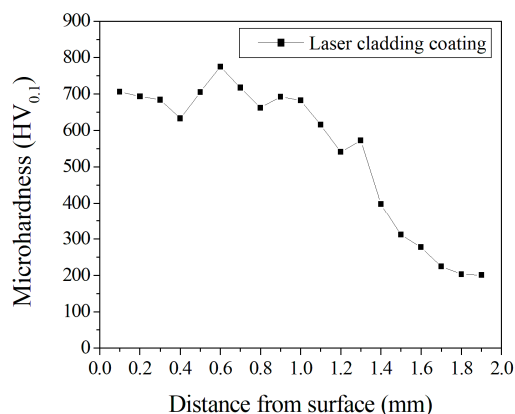


Figure 5. Microhardness distribution of the laser cladding coating.

Figure 6 shows a comparison of the mass wear rates of laser cladding coating and TA2 matrix under dry friction and wear conditions at room temperature. As can be seen from the figure, under the conditions of dry friction loading of 45 N and wear distance of 276.32 m, the mass wear rate of the TA2 matrix is 16.22 mg/min, and that of laser cladding coating is 2.8 mg/min, about 1/5.79 of TA2 matrix. Therefore, the wear resistance of the laser cladding coating is 5.79 times that of the TA2 matrix; that is, the wear resistance of the laser cladding coating is obviously better than that of the TA2 matrix. It is known that the higher the hardness of a material, the better the wear resistance [36]. The average microhardness of the laser cladding coating is 3.34 times that of the TA2 matrix (Figure 5), so the wear resistance of the laser cladding coating is better than that of the TA2 matrix.

It should be pointed out that the improvement factor of wear resistance of the laser cladding coating relative to TA2 matrix is significantly higher than that reported in the literature [37]. In the literature [37], Ti₂SC/TiS composite coating was prepared on TA2

matrix by laser cladding, and the wear rate of TA2 matrix was 3 times that of the composite coating, which was less than 5.79 times that of the coating in this paper.

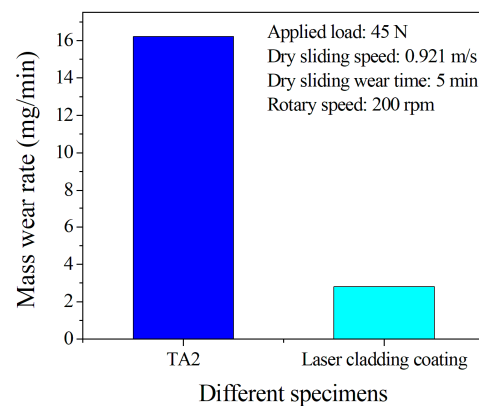


Figure 6. Comparison of mass wear rate between laser cladding coating and TA2 matrix.

Figure 7 shows the SEM morphology of TA2 matrix and laser cladding coating after dry friction and wear. Table 3 shows the EDS results of the worn TA2 matrix and laser cladding coating. According to the SEM morphology of the TA2 matrix after wear in Figure 7a,b, it can be seen that the TA2 matrix after dry friction and wear presents adhesive wear characteristics of being pressed. At the same time, there are deep and wide pear grooves, and there are a large number of fine particles in the grooves. The EDS results in Table 3 show that during dry friction and wear of TA2 matrix, a large number of fine TiO or TiO_x particles are generated due to surface friction heat generation and oxidation. As the abrasive material is SiC with a microhardness of 3200 HV [28], its microhardness is much higher than that of the TA2 matrix. Therefore, under the condition of dry friction and wear, the hard abrasive SiC continuously presses TA2 matrix, causing the surface of the matrix to be scratched and flattened. At the same time, due to the heat generated by dry friction, the Ti in TA2 matrix is oxidized into an incomplete valence TiO_x [38]. Therefore, the main wear mechanisms of TA2 matrix are adhesive wear and oxidative wear.

Table 3. EDS results of worn TA2 matrix and coating.

Different Points	Ti (at.%)	Al (at.%)	Si (at.%)	O (at.%)	Possible Phases
1	91.80	-	-	8.20	Ti + TiO _x
2	51.11	-	-	48.89	TiO
3	100.00	-	-	-	Ti
4	92.11	-	-	7.89	Ti + TiO _x
5	87.00	-	-	13.00	Ti + TiO _x
6	43.34	2.52	24.78	29.36	Ti ₅ Si ₃ + Al ₂ O ₃ + TiO ₂
7	64.69	5.27	30.03	-	Ti ₅ Si ₃ + Ti ₃ Al
8	45.00	2.96	22.99	29.08	Ti ₅ Si ₃ + Al ₂ O ₃ + TiO ₂
9	45.54	2.17	29.40	22.88	Ti ₅ Si ₃ + Al ₂ O ₃ + TiO ₂
10	40.92	2.31	24.37	32.39	Ti ₅ Si ₃ + Al ₂ O ₃ + TiO ₂
11	58.58	14.18	4.80	22.43	Ti ₃ Al + TiO ₂ + SiO ₂

Figure 7c,d show the SEM morphologies of the laser cladding coating after dry friction and wear. Combined with the EDS results in Table 3, it can be seen that after dry friction and wear, furrows of different depths and widths and wear particles of different sizes appear on the surface of the coating. Due to the heat generated by dry friction, most oxidation reactions occur and different oxides are generated, but the furrows of all the coatings are shallow and narrow. The different groove depths and widths of the coating should be closely related to the surface microhardness of the coating, and the different sizes of the coating wear particles should be related to the type and volume fraction of the

intermetallic compounds in the coating. In general, the larger the volume fraction of Ti_5Si_3 phase with higher microhardness in the coating, the smaller the particles, the more severe the abrasive wear of the coating, the more spalling wear particles, the shallower the groove, the lighter the adhesive wear, and the more severe the oxidation wear. However, because the microhardness of the coating is lower than that of the hard anti-abrasive material SiC, abrasive wear, adhesive wear and oxidation wear coexist.

In summary, the wear mechanisms of TA2 matrix are mainly adhesive wear and oxidative wear, whereas the wear mechanisms of coating are abrasive wear, adhesive wear and oxidative wear that co-exist, which is similar to the results reported in the literature [27,39,40].

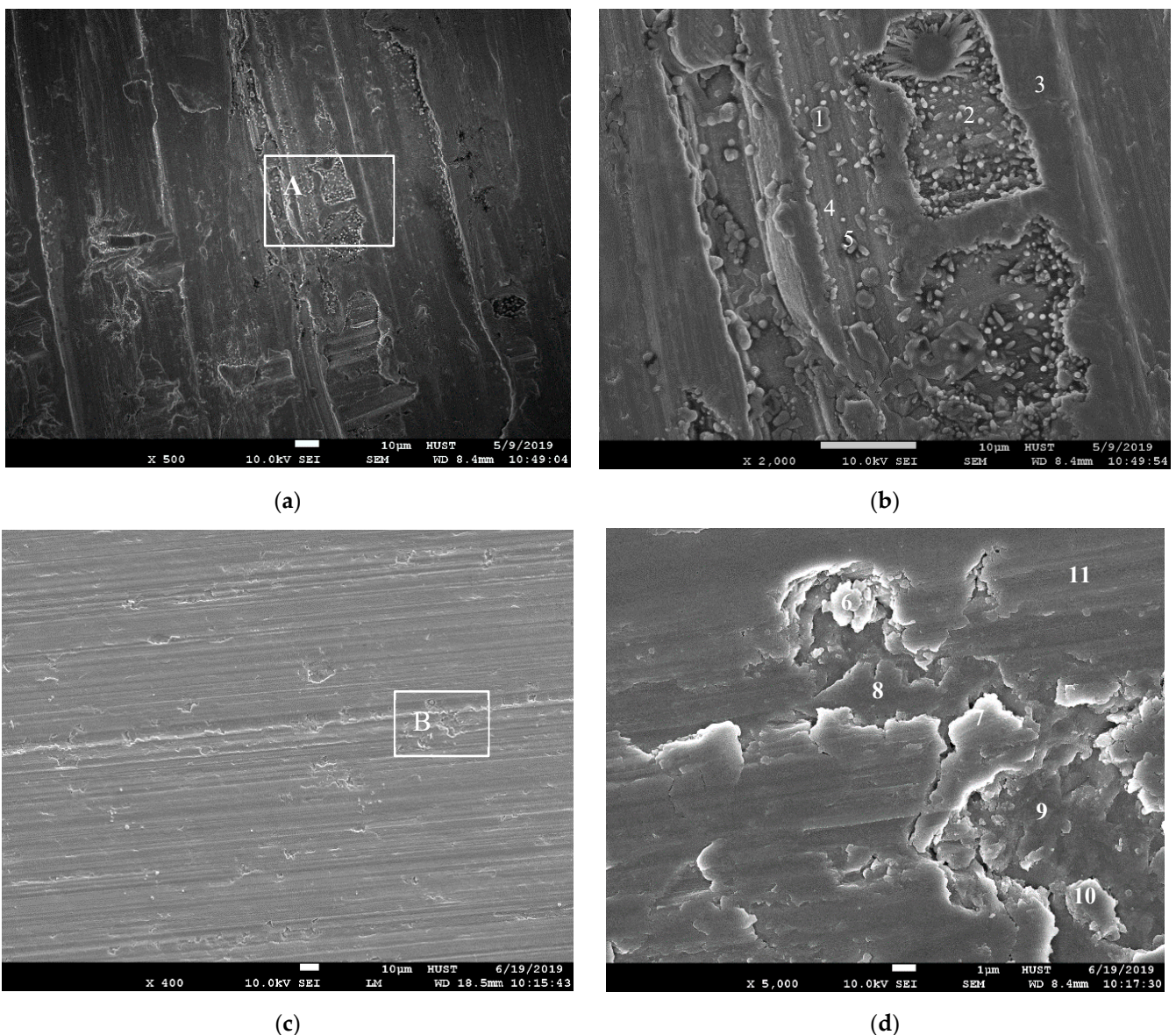


Figure 7. SEM morphology of the worn TA2 matrix and laser cladding coating. (a) Whole SEM morphology of the worn TA2 matrix; (b) local amplified SEM morphology of the worn TA2 matrix in area A in Figure 6a; (c) whole SEM morphology of the worn coating; (d) local amplified SEM morphology of the worn coating in area B in Figure 6c. 1, 2, 3, 4, 5, 6, 7, 8, 9, 10 and 11 in figure represent the location points of the EDS test, respectively.

4. Discussion

4.1. Formation and Flow Characteristics of the Laser Cladding Molten Pool with Double-Layer Preset Powder Layer

As a relatively economical and new surface modification technology, laser cladding can significantly improve the surface properties of substrate materials such as wear resistance, corrosion resistance and oxidation resistance. The laser cladding process is a non-equilibrium, instantaneous and non-uniform physicochemical metallurgical process. The heat conduction and melt flow in the molten pool determine the microstructure, grain morphology and defect types of the cladding layer, thus affecting the properties of the materials and the service life of the parts.

In the case of laser cladding of the double-layer preset powder layer (Figure 1), under the action of the laser beam, the double-layer preset powder layer absorbs the laser energy and melts quickly to form a molten pool. When the laser beam leaves the molten pool, it solidifies quickly. There are three heat transfer modes in this preset laser cladding: heat radiation from the laser to the powder layer, heat convection between the protective gas and powder layer, and heat conduction between the powder layers [41]. These three heat transfer modes lead to complex physical phenomena, such as melting, solidification and phase transformation during laser cladding. Figure 8 shows a schematic diagram of the flow behavior of the cross-section molten pool during laser cladding with a double-layer preset powder layer.

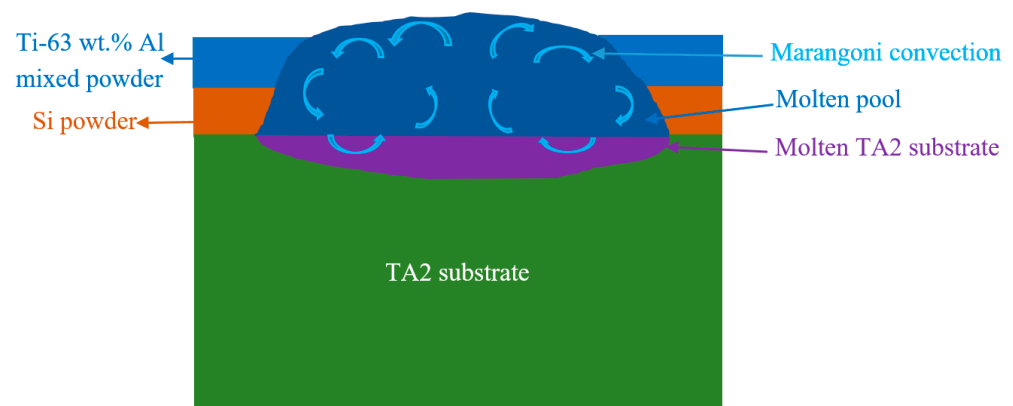


Figure 8. Schematic diagram of flow behavior of cross-section molten pool during laser cladding with double-layer preset powder layer.

During the laser action, the double-layer preset powder layer and part of the substrate melt rapidly due to the absorption of laser energy, forming a large and uneven temperature gradient, resulting in a tension gradient on the surface of the molten pool. Generally, a symmetrical surface tension gradient is generated on the left and right sides of the symmetrical line at the center of the molten pool. Due to the influence of surface tension, the high-temperature melt in the center of the molten pool flows to the surface of the molten pool. At the same time, under the comprehensive action of buoyancy, gravity and other factors, the high-temperature melt flows to both sides along the surface near the center point of the interface. The closer the area is to the edge, the more intense the melt flow and the higher the velocity. Due to the continuity of movement, the low-temperature melt reaching the edge of the molten pool flows along the solid–liquid boundary towards the bottom of the molten pool, and then converges and rises in the middle area of the molten pool, forming the left and right circulating flows of the molten pool (see blue arrows in Figure 8), respectively.

In particular, the change in the surface temperature of the laser molten pool causes a change in the surface tension gradient of the fluid and induces the flow of the surface

fluid from the region of low surface tension to the region of high surface tension. This Marangoni flow is the main driving force for mass transmission in the molten pool [42]:

$$\gamma = \gamma_0 + \sigma(T - T_0)$$

where: γ_0 is the surface tension at the reference temperature T_0 ; σ is the surface tension coefficient.

Moreover, in the process of laser cladding, in addition to the influence of laser cladding process parameters on the temperature field and velocity field of the molten pool, the surface tension coefficient of the material also has an impact on the temperature field and velocity field of the molten pool [43]. When the surface tension coefficient of the material is less than 0, the melt in the molten pool flows from the laser center to the edge of the molten pool. When the material surface tension coefficient is greater than 0, the melt in the molten pool flows from the edge of the molten pool to the laser center, but the peak velocity of both fluid flows appears at the edge of the molten pool surface. The surface tension coefficients of Ti, Si and Al powders used in this paper are -0.16 mN/m, -0.25 mN/m and -0.25 mN/m [44], respectively, which are all negative values, so the flow of the molten pool belongs to the former.

In particular, in the stable zone of the laser cladding layer, the molten pool tends to be stable as the heat input reaches a dynamic equilibrium with the heat lost due to heat transfer. Moreover, under the action of Marangoni flow, the molten double-layer preset powder layer and part of the substrate are mixed and stirred in the molten pool to promote the homogenization of the alloying elements in the molten pool.

In conclusion, under the action of Marangoni flow, Al, Si and Ti alloying elements in the molten pool can be evenly mixed to obtain the effect of laser cladding of a single preset powder layer, and then obtain the laser cladding layer microstructure with basically a uniform composition to ensure the performance and service life of the coating.

4.2. Formation Mechanism of Different Phases in the Coating

In the laser cladding double-layer preset powder layer, once the molten pool is formed, the melted Ti-63 wt.% Al powder layer, the melted Si powder layer and the partially melted TA2 matrix mix with each other under the action of Marangoni flow stirring force. According to the isothermal section diagram of the Ti-Al-Si ternary system at 1000 °C [45], Ti-Al intermetallic compounds and Ti-Si ceramic reinforced phases can be formed by different in situ reactions of Ti, Al and Si powders in different proportions. In addition, according to the Ti-Al binary phase diagram [46], there are mainly TiAl_3 , TiAl_2 , TiAl and Ti_3Al among Ti-Al intermetallic compounds. The melting point of Ti_3Al is 1600 °C, which is higher than that of TiAl_2 (1425 °C), TiAl (1465 °C) and TiAl_3 (1340 °C). According to the Ti-Si binary phase diagram [46], TiSi_2 , TiSi , Ti_5Si_4 , Ti_5Si_3 , Ti_3Si and other compounds can be generated when Ti reacts with Si. The melting point of Ti_5Si_3 is 2130 °C, which is the highest melting point of Ti-Si compounds. In addition, according to the calculation results of Zhu [47], the enthalpy changes in ΔH and Gibbs free energy ΔG of Ti_5Si_3 are the lowest among Ti-Si compounds, so Ti_5Si_3 is the easiest to obtain by solidification first when the composition is appropriate. Si has a low solubility in the Ti-Al phase, and Ti_5Si_3 has a high melting point, so Ti_5Si_3 is the easiest to form in the laser cladding process [48]. Therefore, in this paper, a preset powder scheme was designed according to the location range of the $\text{Ti}_5\text{Si}_3 + \text{Ti}_3\text{Al}$ phase generated in the literature [45], which was finally verified; that is, only the Ti_5Si_3 and Ti_3Al phases were generated in the coating.

4.3. Wear Mechanism of the Coating and TA2 Matrix

As we all know, friction and wear is an extremely complex process. Compared with lubricating friction, dry friction without lubricating medium results in a more intense friction process, more severe wear, and shorter effective working life of friction pairs. The wear amount is a basic parameter that reflects the wear resistance of the material. The smaller the wear amount per unit time, the better the wear resistance. Wear resistance

refers to the ability of the material itself to resist wear damage, and it is usually expressed by the amount of wear. There is a negative correlation between the wear amount and wear resistance; that is, the smaller the wear amount, the better the wear resistance.

The mathematical model of material wear can quantitatively describe the wear process and calculate the normal working life of the friction pairs to better grasp the essence of the wear problem, reduce and control the wear degree, and improve the reliability of the friction pair. In 1953, Archard [49], a professor at the University of Leicester, proposed a computational model for adhesive wear. Archard's wear calculation formula is as follows:

$$Q = k \times (NL)/H$$

where, Q is the amount of adhesive wear on the contact surface; K is the coefficient of adhesive wear, representing the probability of an abrasive particle generated by mutual friction between a pair of micro-convex bodies; N is the normal pressure; H is the hardness of the soft surface materials; L is the relative sliding distance.

Archard's adhesive wear theory describes the general rules of material wear. The wear amount is proportional to the displacement and positive pressure and inversely proportional to the hardness of the softer materials. It connects the wear with the material properties, which makes it convenient to calculate the wear amount. It can be seen that hardness is an important index to evaluate material properties. In general, the higher the hardness, the better the wear resistance of the material.

Specifically in this paper, on the one hand, it can be seen from Figure 5 that the microhardness of the laser cladding coating is higher than that of the TA2 matrix. Therefore, under the same conditions, the wear resistance of the laser cladding coating is better than that of the TA2 matrix (Figure 6).

On the other hand, the wear resistance of materials depends not only on the hardness of the materials but also on the hardness of the abrasives. The microhardness of Ti_5Si_3 , Ti_3Al , TA2 and SiC are 1500HV [28], 530HV_{0.2} [35], 200HV_{0.1} (Figure 5) and 3700HV [28], respectively. Therefore, when the applied load is 45N, it is inevitable that the wear mechanism of the TA2/SiC friction pairs is different from the coating ($Ti_5Si_3 + Ti_3Al$)/SiC friction pairs. That is, although the two groups of friction pairs cause oxidative wear due to the heat generated by dry friction and wear (as evidenced by the appearance of the O element in Table 3) and the hardness difference of the TA2/SiC friction pairs is larger, TA2 is prone to plastic deformation and adhesive wear, whereas the hardness difference of the coating ($Ti_5Si_3 + Ti_3Al$)/SiC friction pairs is relatively small. Ti_5Si_3 (Ti_3Al) is prone to brittle fracture and abrasive wear; however because the hardness of Ti_5Si_3 (Ti_3Al) is lower than that of SiC, adhesive wear also occurs. In conclusion, the TA2/SiC friction pairs mainly exhibit adhesive wear and oxidative wear, whereas the coating($Ti_5Si_3 + Ti_3Al$)/SiC friction pairs mainly exhibit abrasive wear, adhesive wear and oxidative wear.

5. Conclusions

- (1) The wear-resistant Ti_5Si_3/Ti_3Al composite coatings were successfully prepared on TA2 titanium alloy by laser cladding using the double layer preset method of Ti-63 wt.% Al mixed powder layer/Si powder layer.
- (2) The coating is mainly composed of coarse primary Ti_5Si_3 phase and fine Ti_5Si_3/Ti_3Al eutectic structure, with more Ti_5Si_3 on the top layer and in the middle of the coating and more Ti_5Si_3/Ti_3Al eutectic on the bottom.
- (3) The mass wear rate of the laser cladding coating is 1/5.79 of that of the TA2 matrix. The wear mechanisms of the coatings are mainly abrasive wear, adhesive wear and oxidative wear, whereas the wear mechanisms of the TA2 matrix are adhesive wear and oxidative wear.
- (4) The effect of laser cladding of the double preset powder layer is similar to that of the single preset powder layer because of the strong stirring effect of the Marangoni flow in the molten pool.

Author Contributions: Investigation—K.H. and W.H.; writing—original draft preparation, W.H.; writing—review and editing, K.H. All authors have read and agreed to the published version of the manuscript.

Funding: This work was supported by the Open Project Program (No. 2022-KF-19) of the State Key Laboratory of Advanced Technology for Materials Synthesis and Processing, Wuhan University of Technology.

Data Availability Statement: The data of this study are available from the corresponding author upon reasonable request.

Acknowledgments: The authors are grateful to the Analytical and Testing Center of Huazhong University of Science and Technology.

Conflicts of Interest: The authors declare no conflict of interest.

References

1. Budzynski, P.; Kaminski, M.; Surowiec, Z.; Turek, M.; Wiertel, M. Effect of carbon ion implantation and xenon ion irradiation on the tribological properties of titanium and Ti6Al4V Alloy. *Acta Phy. Pol. A* **2022**, *142*, 713–722. [[CrossRef](#)]
2. Zhao, L.D.; Lugscheider, E. Reactive plasma spraying of TiAl6V4 alloy. *Wear* **2002**, *253*, 1214–1218. [[CrossRef](#)]
3. Srinivasan, R.; Kamaraj, M.; Rajeev, D.; Ravi, S.; Senthilkumar, N. Plasma spray coating of aluminum-silicon-MWCNT blends on titanium grade 5 alloy substrate for enhanced wear and corrosion resistance. *Silicon* **2022**, *14*, 8629–8641. [[CrossRef](#)]
4. Koshuro, V.; Fomina, M.; Zakharevich, A.; Fomin, A. Superhard Ta-O-N coatings produced on titanium using induction physical vapor deposition. *Ceram. Int.* **2022**, *48*, 19467–19483. [[CrossRef](#)]
5. Hussein, M.A.; Adesina, A.Y.; Kumar, A.M.; Sorour, A.A.; Ankah, N.; Al-Aqeeli, N. Mechanical, in-vitro corrosion, and tribological characteristics of TiN coating produced by cathodic arc physical vapor deposition on Ti20Nb13Zr alloy for biomedical applications. *Thin Solid Film.* **2020**, *709*, 138183. [[CrossRef](#)]
6. Chen, X.W.; Ren, P.; Zhang, D.F.; Hu, J.; Wu, C.; Liao, D.D. Corrosion and wear properties of h-BN-modified TC4 titanium alloy micro-arc oxide coatings. *Surf. Innov.* **2022**, *11*, 49–59. [[CrossRef](#)]
7. Majumdar, J.D.; Weisheit, A.; Mordike, B.L.; Manna, I. Laser surface alloying of Ti with Si, Al and Si+Al for an improved oxidation resistance. *Mater. Sci. Eng. A* **1999**, *266*, 123–134. [[CrossRef](#)]
8. Wang, Z.; Li, J.N.; Zhang, Z.; Li, J.M.; Su, M.L. Microstructure and wear resistance of Cu/La₂O₃ modified laser clad composites. *Laser. Eng.* **2019**, *44*, 33–39.
9. Ali, S.R.A.S.; Hussein, A.H.A.; Nofal, A.; Elnaby, S.I.H.; Elgazzar, H. A contribution to laser cladding of Ti-6Al-4V titanium alloy. *Metall. Res. Technol.* **2019**, *116*, 634.
10. Tian, Y.; Zhang, Z.; Li, J.N.; Huo, Y.S.; Su, M.L. Surface modification of TA7 titanium alloy with laser clad La₂O₃ amorphous coatings. *Laser. Eng.* **2019**, *44*, 331–339.
11. Li, X.D.; Liu, S.S.; Wang, J.W.; Yu, M.X.; Tang, H.B. Effect of different ZrN addition on microstructure and wear properties of titanium based coatings by laser cladding technique. *Coatings* **2019**, *9*, 261. [[CrossRef](#)]
12. Sui, X.M.; Lu, J.; Zhang, X.; Sun, L.; Zhang, W.P. Microstructure and properties of TiC-reinforced Ti₂Ni/Ti₅Si₃ eutectic-based laser cladding composite coating. *J. Therm. Spray Technol.* **2020**, *29*, 1838–1846. [[CrossRef](#)]
13. Chen, C.N.; Su, M. Study on microstructure and abrasive resistance of laser cladding TiN surface alloyed TC9. *J. Beijing Univ. Aeronaut. Astronaut.* **1998**, *24*, 253–255.
14. Xiang, K.; Chen, L.Y.; Chai, L.J.; Guo, N.; Wang, H. Microstructural characteristics and properties of CoCrFeNiNb_x high-entropy alloy coatings on pure titanium substrate by pulsed laser cladding. *Appl. Surf. Sci.* **2020**, *517*, 146214. [[CrossRef](#)]
15. Wu, H.; Liang, L.X.; Lan, X.D.; Yin, Y.; Song, M.; Li, R.D.; Liu, Y.; Yang, H.O.; Liu, L.; Cai, A.H.; et al. Tribological and biological behaviors of laser clad Ti-based metallic glass composite coatings. *Appl. Surf. Sci.* **2020**, *507*, 145104. [[CrossRef](#)]
16. Chai, L.J.; Wang, C.; Xiang, K.; Wang, Y.Y.; Wang, T.; Ma, Y.L. Phase constitution, microstructure and properties of pulsed laser-clad ternary CrNiTi medium-entropy alloy coating on pure titanium. *Surf. Coat. Technol.* **2020**, *402*, 126503. [[CrossRef](#)]
17. Ke, J.; Liu, X.B.; Liang, J.; Liang, L.; Luo, Y.S. Microstructure and fretting wear of laser cladding self-lubricating anti-wear composite coatings on TA2 alloy after aging treatment. *Opt. Laser Technol.* **2019**, *119*, 105599. [[CrossRef](#)]
18. Guo, C.; Ma, M.L.; Chen, F.; Wei, B.L. Microstructure and space tribological properties of NiCrBSi/Ag composite coating prepared by laser cladding. *Surf. Technol.* **2019**, *48*, 177–184.
19. Guo, C.; Zhou, J.S.; Zhao, J.R.; Wang, L.Q.; Yu, Y.J.; Chen, J.M.; Zhou, H.D. Improvement of the oxidation and wear resistance of pure Ti by laser-cladding Ti₃Al coating at elevated temperature. *Tribol. Lett.* **2011**, *42*, 151–159. [[CrossRef](#)]
20. Zhai, Y.J.; Liu, X.B.; Qiao, S.J.; Wang, M.D.; Lu, X.L.; Wang, Y.G.; Chen, Y.; Ying, L.X. Characteristics of laser clad α-Ti/TiC+(Ti,W)C_{1-x}/Ti₂SC+TiS composite coatings on TA2 titanium alloy. *Opt. Laser Technol.* **2017**, *89*, 97–107. [[CrossRef](#)]
21. Liu, Y.N.; Yang, L.J.; Yang, X.J.; Zhang, T.G.; Sun, R.L. Optimization of microstructure and properties of composite coatings by laser cladding on titanium alloy. *Ceram. Int.* **2021**, *47*, 2230–2243. [[CrossRef](#)]
22. An, Q.; Qi, W.J.; Zuo, X.G. Microstructure and wear resistance of in-situ TiC reinforced Ti-based coating by laser cladding on TA15 titanium alloy surface. *J. Mater. Eng.* **2022**, *50*, 139–146.

23. Ye, Z.Y.; Li, J.N.; Liu, L.Q.; Ma, F.K.; Zhao, B.; Wang, X.L. Microstructure and wear performance enhancement of carbon nanotubes reinforced composite coatings fabricated by laser cladding on titanium alloy. *Opt. Laser Technol.* **2021**, *139*, 106957. [[CrossRef](#)]
24. Maliutina, I.N.; Si-Mohand, H.; Sijobert, J.; Lazurenkoa, D.V.; Bataev, I.A. Structure and oxidation behavior of γ -TiAl coating produced by laser cladding on titanium alloy. *Surf. Coat. Technol.* **2017**, *319*, 136–144. [[CrossRef](#)]
25. Weng, F.; Yu, H.J.; Liu, J.L.; Chen, C.Z.; Dai, J.J.; Zhao, Z.H. Microstructure and wear property of the Ti_5Si_3/TiC reinforced Co-based coatings fabricated by laser cladding on Ti-6Al-4V. *Opt. Laser Technol.* **2017**, *92*, 156–162. [[CrossRef](#)]
26. Jiang, P.; Zhang, J.J.; Yu, L.G.; Wang, H.M. Wear-resistant Ti_5Si_3/TiC composite coatings made by laser surface alloying. *Rare Metal Mater. Eng.* **2000**, *29*, 269–272.
27. Guo, C.; Zhou, J.S.; Chen, J.M.; Zhao, J.R.; Yu, Y.J.; Zhou, H.D. Improvement of the oxidation and wear resistance of pure Ti by laser cladding at elevated temperature. *Surf. Coat. Technol.* **2010**, *205*, 2142–2151. [[CrossRef](#)]
28. Zhang, H.X. Investigation on Microstructure and Wear Resistance of Ti-Al-Si Ceramic Composite Coatings on Titanium Alloys by Laser Cladding. Ph.D. Thesis, Shandong University, Jinan, China, 2016.
29. Vojtěch, D.; Novák, M.; Novák, P.; Lejček, P.; Kopeček, J. Unidirectional crystallization and high-temperature oxidation of in situ $Ti_3(Al,Si)-Ti_5(Si,Al)_3$ composite. *Mater. Sci. Eng. A* **2008**, *489*, 1–10. [[CrossRef](#)]
30. Wu, J.S.; Qiu, G.H.; Zhang, L.T. The β -Ti(Al,Si)+ $Ti_5(Si,Al)_3$ eutectic line in the Ti-Al-Si ternary system. *Mater. Sci. Technol.* **1994**, *2*, 1–7. (In Chinese)
31. Wu, J.S.; Beaven, P.A.; Wagner, R. The $Ti_3(Al,Si)+Ti_5(Si,Al)_3$ eutectic reaction in the Ti-Al-Si system. *Scr. Metall. Mater.* **1990**, *24*, 207–212. [[CrossRef](#)]
32. Wu, J.S.; Qiu, G.H.; Zhang, L.T. The β -Ti(Al,Si)+ $Ti_5(Si,Al)_3$ eutectic line in the Ti-Al-Si ternary system. *Scr. Metall. Mater.* **1994**, *30*, 213–218. [[CrossRef](#)]
33. Liu, J.L.; Zou, Z.R.; Su, B.R. *High Energy Beam Heat Treatment*; China Machine Press: Beijing, China, 1997; pp. 40–46.
34. Jackson, M.J.; Robinson, G.M.; Gill, M.D.H.; Neill, W.O. The effect of nozzle design on laser micro-machining of M2 tool steels. *J. Mater. Process. Technol.* **2005**, *160*, 198–212. [[CrossRef](#)]
35. Guo, C.; Chen, J.M.; Yao, R.G.; Zhou, J.S.; Zhang, S.T. Microstructure and tribological properties of Ti_3Al intermetallic compound coating prepared by laser cladding. *Tribol. Lett.* **2013**, *33*, 14–21.
36. Wang, Y.; Xiong, J.; Yan, J.; Fan, H.Y.; Wang, J. Oxidation resistance and corrosion behavior of hot-dip aluminized coatings on commercial-purity titanium. *Surf. Coat. Technol.* **2011**, *206*, 1277–1282. [[CrossRef](#)]
37. Shi, G.N.; Wu, S.H.; Lu, X.L.; Liu, X.B. Microstructure and property of laser clad Ti_2SC/TiS self-lubricating anti-wear composite coating on TA2 titanium alloy. *Trans. Mater. Heat Treat.* **2016**, *37*, 198–202.
38. Okamoto, H. O-Ti (Oxygen-Titanium). *J. Phase Equilibria Diffus.* **2011**, *32*, 473–474. [[CrossRef](#)]
39. Yu, P.C.; Liu, X.B.; Liu, X.L.; Zhu, G.X.; Chen, Y.; Wu, S.H. Study on tribology and high-temperature oxidation resistance of laser cladding composite coatings on Ti6Al4V alloy. *Chin. J. Lasers* **2015**, *42*, 81–88.
40. Yu, J.J.; Zhang, X.Y.; Ma, L.L.; Li, H.; Zou, L.J.; Zhang, W.P. Microstructures and properties of laser cladding Ti/Ni+ Si_3N_4/ZrO_2 composite coatings on TA15 titanium alloys. *Surf. Technol.* **2016**, *45*, 105–109.
41. Cui, Z.Y.; Fang, C.; Zhang, W.L. Effects of Marangoni flow on the thermal behavior and melt flow behavior in laser cladding. *Appl. Laser* **2018**, *38*, 409–416.
42. Lee, Y.S.; Nordin, M.; Babu, S.S.; Farson, D.F. Influence of fluid convection on weld pool formation in laser cladding. *Weld. J.* **2014**, *93*, 292–300.
43. Zhao, M.J.; Li, B.X.; Wu, T.; Zhao, L.Z.; Zeng, J.B.; Jiao, H.T.; Li, J.; Song, L.J. Study on the effect mechanism of laser cladding velocity field based on thermal-fluid coupling model. *J. East China Jiaotong Univ.* **2022**, *39*, 74–83.
44. Mills, K.C.; Su, Y.C. Review of surface tension data for metallic elements and alloys: Part 1—Pure metals. *Int. Mater. Rev.* **2006**, *51*, 329–351. [[CrossRef](#)]
45. Raghavan, V. Al-Si-Ti (Aluminum-Silicon-Titanium). *J. Phase Equilibria Diffus.* **2009**, *30*, 82–83. [[CrossRef](#)]
46. ASM International. *ASM Metals Handbook Volume 3-Alloy Phase Diagrams*; The Materials Information Company: Houston, TX, USA, 1992; pp. 327, 1420.
47. Zhu, Y.; Yang, Y.Q.; Ma, Z.J.; Chen, Y. Thermodynamic studies on interfacial reactions in SiC-fibre-reinforced Ti-matrix composites. *Rare Met. Mater. Eng.* **2002**, *31*, 279–282.
48. Vojtěch, D.; Novák, M.; Novák, P.; Kopeček, J.; Guhlová, P. Properties of (Ti,Nb)Al-(Ti,Nb)Si eutectic composite. *Compos. Struct.* **2010**, *92*, 1440–1448. [[CrossRef](#)]
49. Archard, J.F. Contact and rubbing of flat surfaces. *J. Appl. Phys.* **1953**, *24*, 981–988. [[CrossRef](#)]

Disclaimer/Publisher’s Note: The statements, opinions and data contained in all publications are solely those of the individual author(s) and contributor(s) and not of MDPI and/or the editor(s). MDPI and/or the editor(s) disclaim responsibility for any injury to people or property resulting from any ideas, methods, instructions or products referred to in the content.